Advantage of nonlinear relativistic mean-field model in studying neutron star matter

K. Miyazaki

E-mail: miyazakiro@rio.odn.ne.jp

Abstract

We test the extended Zimanyi-Moszkowski model of relativistic nuclear matter for reproducing the density dependence of the symmetry energy, the direct URCA constraint $M_G^{DU} \geq 1.5M_\odot$ on the gravitational mass of neutron star (NS), the large radii of NSs in RX J1856.5-3754 and qLMXB X7, the massive NSs in PSR J0751+1807 and 4U1700-37, and the baryonic mass of J0737-3039B. The two sets of $NN\rho$ coupling constant are considered. The first (EZM1) is the same as the Bonn A potential. The second (EZM2) is chosen so as to reproduce the symmetry energy $E_s = 32\,\mathrm{MeV}$ of nuclear matter. The EZM1 can pass 6 tests among 7, while the EZM2 passes 5 tests. We can therefore conclude that the EZM model has unique and excellent features and is the most prospective one for studying the dense baryonic matter.

1 Introduction

To study the equation-of-state (EOS) of dense nuclear medium has been an important subject in nuclear physics and astrophysics. It becomes more and more important as increasing information from the intermediate-energy heavy-ion experiments and the astronomical observations of neutron stars (NSs). Although whether the EOS is stiff or soft is a controversial problem until now, the recent noticeable observations of the nearby isolated NS RX J1856-3754 [1] and the quiescent low-mass X-ray binary (qLMXB) X7 [2] have strongly suggested that the NSs of the typical gravitational masses $M_G = 1.4M_\odot \sim 1.5M_\odot$ hold larger radii than 13 km. This indicates that the stiff EOS is favorable and so severely restricts the models of dense nuclear matter. In fact, the EOS from the extensive variational calculation [3], which has no fitting parameters and so is believed to be most reliable, has been ruled out. Moreover, the possibilities of (strange) quark stars and quark matter cores have been denied.

Consequently, there remain the relativistic models based on the field theory of nucleons interacting through mesons [4] as possible candidates to reproduce the reasonable EOS of NS matter. In this respect, the latest paper [5] has performed extensive tests of the EOSs in several relativistic models, which are the so-called nonlinear Walecka (NLW) model

[6], the Dirac-Brueckner-Hartree-Fock (DBHF) model [7], the density-dependent (DD) relativistic mean-field (RMF) model [8] and the truly nonlinear RMF model developed recently by Kolomeitsev and Voskresensky (KV) [9]. Here it is noted that the KV model has nonlinear meson-nucleon couplings, while the NLW model does not so in spite of its name.

The truly nonlinear RMF model was first developed by Zimanyi-Moszkowski (ZM) [10]. The KV model can be regarded as an extension of the ZM model. On the other hand, Ref. [11] developed another nonlinear model in a completely different point of view from the ZM model. The physical origin of the ZM model was also investigated in Refs. [12] and [13]. Moreover, the present author found [14] that the ZM model can be interpreted in the constituent quark model of nucleons and that a little modification of it reproduces the same saturation properties of nuclear matter as the DBHF model in Ref. [15]. (But it is different from the result of Tübingen group [7].) This extended Zimanyi-Moszkowski (EZM) model has no more free parameters than the $NN\sigma$ and $NN\omega$ coupling constants, which are adjusted so as to reproduce the saturation, in contrast to the DD and KV models. Moreover, their values are close to those in Bonn A potential [15]. Therefore, the applications of the EZM model to asymmetric matter [16] and dense hadronic matter containing strangeness [14,17-23] are possible without ambiguities.

Although the NS matter in the EZM model has already been investigated in Ref. [16], there was used an approximation [24] in the numerical calculation. In the present paper, we will reinvestigate the NS matter in the EZM model through the exact calculation. Because the EZM model is not familiar, our main purpose is to supplement the extensive tests of RMF models in Ref. [5] with the EZM model and to show its unique and excellent feature. In the next section, the EZM model of NS matter is reviewed. In section 3 we impose the similar extensive tests to Ref. [15] on it. Finally, the results are discussed and our conclusions are derived in section 4.

2 The EZM model of NS matter

Here we reformulate the EZM model of NS matter in a somewhat different fashion from Ref. [16]. In the present work we consider only nucleons as baryons so as to compare the EZM model with the results in Ref. [5]. The model Lagrangian for NS matter in the mean-field approximation is

$$\begin{aligned}\mathcal{L} &= \sum_{N=p,\,n} \bar{\psi}_N \left(\not{p} - M_N^* - \gamma^0 V_N \right) \psi_N + \sum_{l=e^-,\,\mu^-} \bar{\psi}_l \left(\not{p} - m_l \right) \psi_l \\ &\quad - \frac{1}{2} m_\sigma^2 \langle \sigma \rangle^2 - \frac{1}{2} m_\delta^2 \langle \delta_3 \rangle^2 + \frac{1}{2} m_\omega^2 \langle \omega_0 \rangle^2 + \frac{1}{2} m_\rho^2 \langle \rho_{03} \rangle^2 , \end{aligned} \tag{1}$$

where ψ_N and ψ_l are the Dirac fields of nucleons and leptons. The isoscalar-scalar, isoscalar-vector, isovector-scalar and isovector-vector mean-fields are $\langle \sigma \rangle$, $\langle \omega_0 \rangle$, $\langle \delta_3 \rangle$ and

$\langle\rho_{03}\rangle$, respectively. The masses of each meson are m_σ, m_ω, m_δ and m_ρ. The renormalized mass of nucleon M_N^* in the matter is defined by

$$M_N^* = m_N^* M_N = M_N + S_N. \tag{2}$$

The scalar potentials are

$$S_p = -g_{pp\sigma}^* \langle\sigma\rangle - g_{pp\delta}^* \langle\delta_3\rangle , \tag{3}$$

$$S_n = -g_{nn\sigma}^* \langle\sigma\rangle + g_{nn\delta}^* \langle\delta_3\rangle , \tag{4}$$

while the vector potentials are

$$V_p = g_{pp\omega}^* \langle\omega_0\rangle + g_{pp\rho}^* \langle\rho_{03}\rangle , \tag{5}$$

$$V_n = g_{nn\omega}^* \langle\omega_0\rangle - g_{nn\rho}^* \langle\rho_{03}\rangle . \tag{6}$$

The renormalized coupling constants in Eqs. (3)-(6) are given [14,16] by

$$g_{pp\sigma(\omega)}^* \equiv h_{pp\sigma(\omega)}^* g_{NN\sigma(\omega)} = \left[(1-\lambda) + \lambda\, m_p^*\right] g_{NN\sigma(\omega)}, \tag{7}$$

$$g_{nn\sigma(\omega)}^* \equiv h_{nn\sigma(\omega)}^* g_{NN\sigma(\omega)} = \left[(1-\lambda) + \lambda\, m_n^*\right] g_{NN\sigma(\omega)}, \tag{8}$$

$$g_{pp\delta(\rho)}^* \equiv h_{pp\delta(\rho)}^* g_{NN\delta(\rho)} = \left[(1-\lambda) + \lambda\left(2m_n^* - m_p^*\right)\right] g_{NN\delta(\rho)}, \tag{9}$$

$$g_{nn\delta(\rho)}^* \equiv h_{nn\delta(\rho)}^* g_{NN\delta(\rho)} = \left[(1-\lambda) + \lambda\left(2m_p^* - m_n^*\right)\right] g_{NN\delta(\rho)}, \tag{10}$$

where $g_{NN\sigma(\omega,\delta,\rho)}$ is the free coupling constant and $\lambda = 1/3$.

The total energy density of NS matter is given by

$$\begin{aligned}\mathcal{E} \;=\; & \frac{1}{4}\sum_{N=p,\,n} \left(\, 3E_{FN}^* \rho_N + M_N^* \rho_{SN}\right) + \frac{1}{4}\sum_{l=e^-,\,\mu^-} \left(\, 3E_{Fl}\rho_l + m_l \rho_{Sl}\right) + \sum_{N=p,\,n} V_N \rho_N \\ & + \frac{1}{2}\, m_\sigma^2 \langle\sigma\rangle^2 + \frac{1}{2}\, m_\delta^2 \langle\delta_3\rangle^2 - \frac{1}{2}\, m_\omega^2 \langle\omega_0\rangle^2 - \frac{1}{2}\, m_\rho^2 \langle\rho_{03}\rangle^2 ,\end{aligned} \tag{11}$$

where ρ_N and ρ_l are the vector densities of baryons and leptons in NS matter, E_{FN}^* and E_{Fl} are their Fermi energies, and ρ_{SN} and ρ_{Sl} are their scalar densities. From Eqs. (2)-(4) the scalar mean-fields $\langle\sigma\rangle$ and $\langle\delta_3\rangle$ are expressed by the renormalized nucleon masses M_p^* and M_n^*. From Eqs. (5) and (6) the vector mean-fields $\langle\omega_0\rangle$ and $\langle\rho_{03}\rangle$ are expressed by the vector potentials V_p and V_n. The total energy density $\mathcal{E}$ of Eq. (11) is therefore expressed by M_N^* and V_N. Then, they are determined by extremizing the energy, $\partial\mathcal{E}/\partial M_N^* = 0$ and $\partial\mathcal{E}/\partial V_N = 0$. Consequently, we have the self-consistency equations:

$$\frac{\rho_p}{M_N}\left(C^{(0)}\right)^2-\left[\left(\frac{m_\omega}{g_{NN\omega}}\right)^2\left(h^*_{nn\rho}\right)^2+\left(\frac{m_\rho}{g_{NN\rho}}\right)^2\left(h^*_{nn\omega}\right)^2\right]v_p$$
$$-\left[\left(\frac{m_\omega}{g_{NN\omega}}\right)^2 h^*_{pp\rho}h^*_{nn\rho}-\left(\frac{m_\rho}{g_{NN\rho}}\right)^2 h^*_{pp\omega}h^*_{nn\omega}\right]v_n=0, \tag{12}$$

$$\frac{\rho_n}{M_N}\left(C^{(0)}\right)^2-\left[\left(\frac{m_\omega}{g_{NN\omega}}\right)^2 h^*_{pp\rho}h^*_{nn\rho}-\left(\frac{m_\rho}{g_{NN\rho}}\right)^2 h^*_{pp\omega}h^*_{nn\omega}\right]v_p$$
$$-\left[\left(\frac{m_\omega}{g_{NN\omega}}\right)^2\left(h^*_{pp\rho}\right)^2+\left(\frac{m_\rho}{g_{NN\rho}}\right)^2\left(h^*_{pp\omega}\right)^2\right]v_n=0, \tag{13}$$

$$\frac{\rho_{Sp}}{M_N}\left(C^{(0)}\right)^3+\left(\frac{m_\sigma}{g_{NN\sigma}}\right)^2 A^{(0)}\left(A^{(1)}_p C^{(0)}-A^{(0)}C^{(1)}_p\right)+\left(\frac{m_\delta}{g_{NN\delta}}\right)^2 B^{(0)}\left(C^{(0)}-B^{(0)}C^{(1)}_p\right)$$
$$-\lambda\left(\frac{m_\omega}{g_{NN\omega}}\right)^2\left(h^*_{nn\rho}v_p+h^*_{pp\rho}v_n\right)\left\{\left[h^{*2}_{pp\rho}-h^{*2}_{nn\rho}+h^*_{pp\omega}h^*_{pp\rho}+h^*_{nn\omega}h^*_{nn\rho}\right]v_p\right.$$
$$\left.-\left[\left(h^*_{pp\omega}+h^*_{pp\rho}\right)h^*_{nn\rho}+\left(h^*_{nn\omega}+h^*_{nn\rho}\right)h^*_{pp\rho}\right]v_n\right\}$$
$$+\lambda\left(\frac{m_\rho}{g_{NN\rho}}\right)^2\left(h^*_{nn\omega}v_p-h^*_{pp\omega}v_n\right)\left[2h^*_{nn\omega}h^*_{nn\rho}v_p+\left(h^*_{nn\omega}h^*_{pp\rho}-h^*_{pp\omega}h^*_{nn\rho}\right)v_n\right]=0, \tag{14}$$

$$\frac{\rho_{Sn}}{M_N}\left(C^{(0)}\right)^3+\left(\frac{m_\sigma}{g_{NN\sigma}}\right)^2 A^{(0)}\left(A^{(1)}_n C^{(0)}-A^{(0)}C^{(1)}_n\right)-\left(\frac{m_\delta}{g_{NN\delta}}\right)^2 B^{(0)}\left(C^{(0)}+B^{(0)}C^{(1)}_n\right)$$
$$-\lambda\left(\frac{m_\omega}{g_{NN\omega}}\right)^2\left(h^*_{nn\rho}v_p+h^*_{pp\rho}v_n\right)\left\{\left[h^{*2}_{nn\rho}-h^{*2}_{pp\rho}+h^*_{pp\omega}h^*_{pp\rho}+h^*_{nn\omega}h^*_{nn\rho}\right]v_n\right.$$
$$\left.-\left[\left(h^*_{pp\omega}+h^*_{pp\rho}\right)h^*_{nn\rho}+\left(h^*_{nn\omega}+h^*_{nn\rho}\right)h^*_{pp\rho}\right]v_p\right\}$$
$$-\lambda\left(\frac{m_\rho}{g_{NN\rho}}\right)^2\left(h^*_{nn\omega}v_p-h^*_{pp\omega}v_n\right)\left[2h^*_{pp\omega}h^*_{pp\rho}v_n+\left(h^*_{pp\omega}h^*_{nn\rho}-h^*_{pp\rho}h^*_{nn\omega}\right)v_p\right]=0, \tag{15}$$

where we have introduced $V_{p(n)}=v_{p(n)}M_N$ and

$$A^{(0)}=h^*_{nn\delta}\left(m^*_p-1\right)+h^*_{pp\delta}\left(m^*_n-1\right), \tag{16}$$

$$B^{(0)}=h^*_{nn\sigma}\left(m^*_p-1\right)-h^*_{pp\sigma}\left(m^*_n-1\right), \tag{17}$$

$$C^{(0)}=h^*_{pp\sigma}h^*_{nn\delta}+h^*_{nn\sigma}h^*_{pp\delta}=h^*_{pp\omega}h^*_{nn\rho}+h^*_{nn\omega}h^*_{pp\rho}, \tag{18}$$

$$A_p^{(1)} = (1-2\lambda) + 2\lambda\left(2m_p^* - m_n^*\right), \tag{19}$$

$$C_p^{(1)} = 2\lambda\, h_{nn\delta}^*, \tag{20}$$

$$A_n^{(1)} = (1-2\lambda) + 2\lambda\left(2m_n^* - m_p^*\right), \tag{21}$$

$$C_n^{(1)} = 2\lambda\, h_{pp\delta}^*. \tag{22}$$

The baryon and scalar densities in Eqs. (12)-(15) are determined from the chemical potentials μ_p and μ_n of nucleons through their Fermi momenta k_{Fp} and k_{Fn}:

$$\mu_N = \left(k_{FN}^2 + M_N^{*\,2}\right)^{1/2} + V_N. \tag{23}$$

Because the NS matter satisfies the β-equilibrium condition

$$\mu_n - \mu_p = \mu_e = \mu_\mu, \tag{24}$$

there are only two independent chemical potentials, which are constrained by the baryon number conservation

$$\rho_B = \rho_p + \rho_n, \tag{25}$$

and the charge neutral condition

$$\rho_p = \rho_e + \rho_\mu. \tag{26}$$

3 Tests of the EZM model

For calculating in RMF model, we have to specify the meson-nucleon coupling constants. The $NN\sigma$ and $NN\omega$ coupling constants, $(g_{NN\sigma}/m_\sigma)^2 = 16.9\,\mathrm{fm}^2$ and $(g_{NN\omega}/m_\omega)^2 = 12.5\,\mathrm{fm}^2$, have been determined [14] so as to reproduce the nuclear matter saturation. The $NN\delta$ coupling constant $(g_{NN\delta}/m_\delta)^2 = 0.39\,\mathrm{fm}^2$ is assumed to be the same as the Bonn A potential in Ref. [15]. On the other hand, we consider two sets of the $NN\rho$ coupling constant. The first one $(g_{NN\rho}/m_\rho)^2 = 0.82\,\mathrm{fm}^2$, referred as EZM1, is also same as the Bonn A potential, while the second one $(g_{NN\rho}/m_\rho)^2 = 1.433\,\mathrm{fm}^2$, referred as EZM2, is determined so as to reproduce the empirical symmetry energy of nuclear matter $E_s = 32.0\,\mathrm{MeV}$ [25]. Although the isovector part of EZM1 is free from parameters, its symmetry energy $E_s = 24.6\,\mathrm{MeV}$ is rather low.

Once determining the coupling constants, for a definite density ρ_B in Eq. (25) we can solve the selfconsistent equations (12)-(15), (25) and (26) in terms of 6-dimensional Newton-Raphson method so that the renormalized masses M_p^* and M_n^*, the vector potentials V_p and V_n, and the chemical potentials μ_p and μ_n are calculated. We first show in Fig. 1 the pressures of NS matter as functions of the total baryon density. The pressure is calculated in terms of the Gibbs-Duhem relation $P = \mu_n\rho_B - \mathcal{E}$. The black and red curves are the results of EZM1 and EZM2, respectively. The region enclosed by the blue

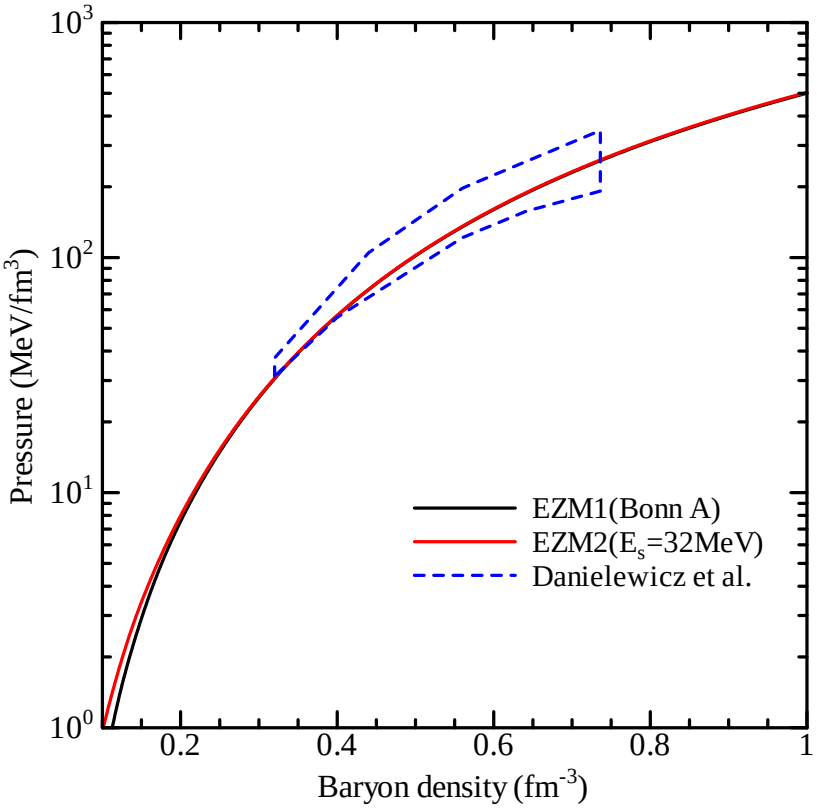

Figure 1: The pressures of NS matter as functions of the total baryon density. The black and red curves are the results of EZM1 and EZM2, respectively. The region enclosed by the blue dashed lines shows the empirical values for pure neutron matter in Ref. [26].

dashed lines shows the empirical values of Fig. 5 in Ref. [26] for pure neutron matter, which are consistent with the experimental flow data from heavy-ion reactions. Although the NS matter is not a pure neutron matter, it is highly asymmetric as seen below in Fig. 2. The empirical values of the pressure for NS matter are therefore expected to be only slightly lower than those in Fig. 1. Consequently, we can conclude that both the EZM models reproduce the empirical values well. To the contrary, Ref. [5] calculates the pressures of symmetric nuclear matter rather than NS matter and compares them with the empirical values of Fig. 3 in Ref. [26] rather than Fig. 5. For symmetric matter, the pressure in the EZM model is somewhat larger than the upper boundary of the empirical values. This is because the incompressibility $K = 302\,\mathrm{MeV}$ of the EZM model is higher than the values of the other RMF models in Ref. [5]. However, $K = 300\,\mathrm{MeV}$ is still reasonable in the analyses of Ref. [26]. Therefore, the pressure of symmetric nuclear matter cannot be a meaningful criterion to constrain the models.

In Fig. 1 there is little difference between EZM1 and EZM2. This indicates that the contribution of ρ mean-field to the pressure of dense nuclear matter is not significant. The difference in $NN\rho$ coupling constant is however apparent in the density dependence of the symmetry energy $E_s(\rho_B)$, which can be expanded around the nuclear matter saturation

Table 1: The values L and $K_{asy} \equiv K_s - 6L$ in Eqs. (27)-(29) from the EZM models and their empirical values derived from isospin diffusion in heavy-ion reactions. The first empirical value is suggested by the authors of Refs. [27] and [28]. The second is the value that the present author finds directly from Fig. 4 in Ref. [27] and Fig. 8 in Ref. [28].

	EZM1	EZM2	Empirical 1	Empirical 2
L(MeV)	65.0	88.8	88 ± 22	$70 \leq L \leq 105$
K_{asy}(MeV)	-369	-529	-500 ± 50	$-550 \leq K_{asy} \leq -500$

density ρ_0 as

$$E_s(\rho_B) = E_s(\rho_0) + \frac{L}{3}\left(\frac{\rho_B - \rho_0}{\rho_0}\right) + \frac{K_s}{18}\left(\frac{\rho_B - \rho_0}{\rho_0}\right)^2, \tag{27}$$

where

$$L = 3\rho_0 \left.\frac{\partial E_s(\rho_B)}{\partial \rho_B}\right|_{\rho_B=\rho_0}, \tag{28}$$

$$K_s = 9\rho_0^2 \left.\frac{\partial^2 E_s(\rho_B)}{\partial \rho_B^2}\right|_{\rho_B=\rho_0}. \tag{29}$$

The L and K_s determine the behavior of the symmetry energy at high densities if the higher order terms than $[(\rho_B - \rho_0)/\rho_0]^3$ are neglected in Eq. (27). We compare in Table 1 the calculated values of L and $K_{asy} \equiv K_s - 6L$ in the EZM models with their empirical values [27,28] derived from isospin diffusion data in heavy-ion reactions. We show two sets of empirical values. The first is the value suggested by the authors of Refs. [27] and [28]. The second is the value that the present author finds directly from Fig. 4 in Ref. [27] and Fig. 8 in Ref. [28]. This is because the margins of the first set seem to be artificially loosed. In any case the EZM2 reproduces the empirical values well while the EZM1 fails.

Next, we show in Fig. 2 the proton fractions of NS matter. The black and red solid curves are the results of EZM1 and EZM2, respectively. Because the ρ mean-field $\langle\rho_{03}\rangle$ is negative in NS matter, the stronger $NN\rho$ coupling constant leads to weaker vector potential V_p in Eq. (5). The weaker V_p leads to higher Fermi momentum k_{Fp} in Eq. (23). Therefore, the EZM2 produces richer protons than the EZM1. According to the standard scenario of NS cooling, the direct URCA process should be suppressed. This implies [5] that in the NSs of lower masses than the typical gravitational mass $M_G = 1.5M_\odot$ the direct URCA cooling is forbidden. In order to investigate this direct URCA constraint in the EZM models, the lowest limit on the proton fraction, above which the rapid cooling through the direct URCA happens, is calculated:

$$f_p^{DU} = \frac{1}{1 + (1 + k_{Fe}/k_{Fp})^3}, \tag{30}$$

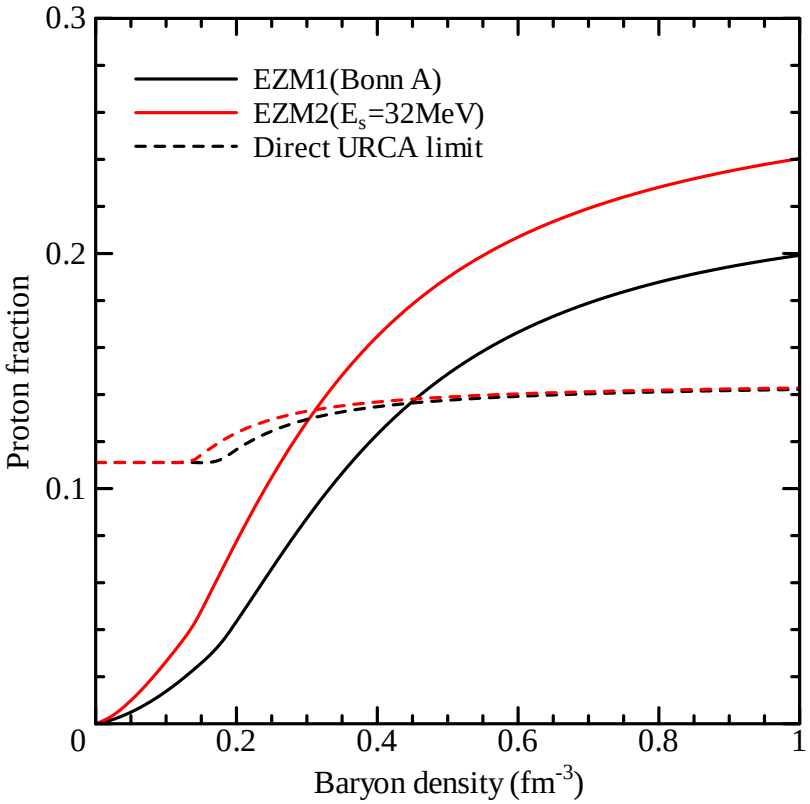

Figure 2: The proton fractions (the solid curves) and their Direct URCA limits (the dashed curves) of NS matter in the EZM1 (the black curves) and the EZM2 (the red curves) as functions of the baryon density.

where k_{Fe} is the Fermi momentum of electron. The results are shown by the dashed curves. The intersection between the solid and dashed curves determines the direct URCA limit on the central density ρ_B^{DU} and so the gravitational mass M_G^{DU} of NS. Because of the charge neutral condition (26), the ratio k_{Fe}/k_{Fp} in Eq. (30) does not strongly depend on the proton fraction and so there is little difference between the direct URCA limits in EZM1 and EZM2. Consequently, $\rho_B^{DU} = 0.447\,\mathrm{fm}^{-3}$ in the EZM1 is higher than $\rho_B^{DU} = 0.312\,\mathrm{fm}^{-3}$ in the EZM2. The gravitational mass (and the radius in Fig. 4) of NS is calculated by integrating the Tolman-Oppenheimer-Volkov equation [29]. For the crust of NS in low-density region $\rho_B < 0.1\,\mathrm{fm}^{-3}$, we use the EOSs by Feynman-Metropolis-Teller, Baym-Pethick-Sutherland and Negele-Vautherin from Ref. [30]. Figure 3 shows the gravitational masses as functions of the central baryon density in NS. There is little difference between the EZM1 (the black curve) and the EZM2 (the red curve) because the pressures of both the models are almost the same as seen in Fig. 1. For a definite central density the mass of NS in the EZM model is heavier than the other RMF models in Ref. [5]. This is because as mentioned above the incompressibility of the EZM model is higher than those of the other models. The dashed lines indicate the direct URCA limits on the gravitational masses corresponding to ρ_B^{DU} determined above. We have

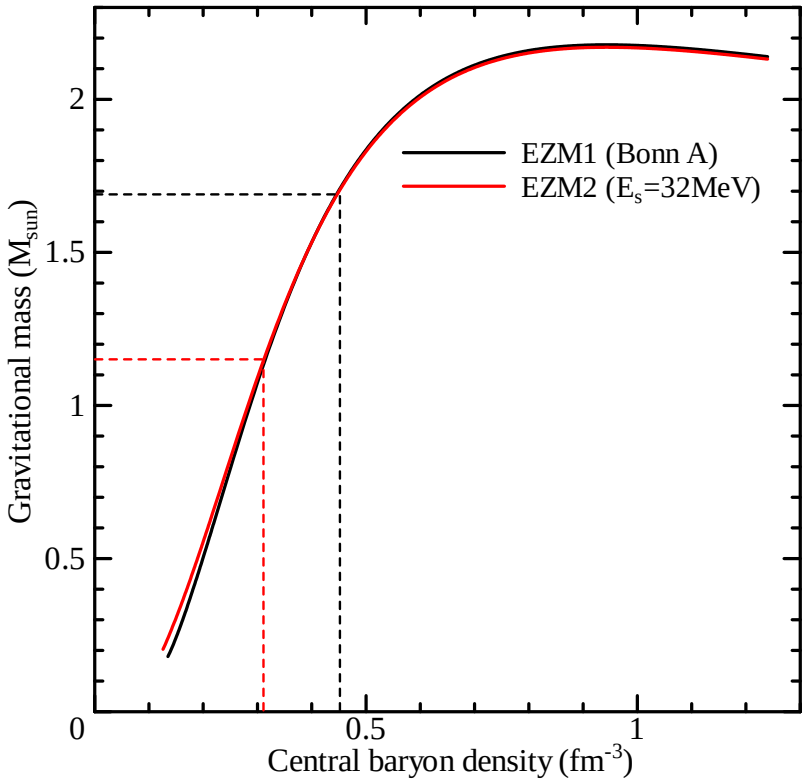

Figure 3: The gravitational masss of NSs as functions of their central baryon densities. The black and red solid curves are the results of EZM1 and EZM2, respectively. The dashed lines indicate the direct URCA limits on the gravitational masses corresponding to $\rho_B^{DU} = 0.447\,\mathrm{fm}^{-3}$ in the EZM1 and $\rho_B^{DU} = 0.312\,\mathrm{fm}^{-3}$ in the EZM2.

$M_G^{DU} = 1.69M_\odot$ in the EZM1 and $M_G^{DU} = 1.15M_\odot$ in the EZM2. The EZM1 satisfies the direct URCA constraint $M_G^{DU} \geq 1.5M_\odot$ but the EZM2 can not. It is seen that the direct URCA constraint is not consistent to the constraint on the symmetry energy in Table 1. In general, the constraints on the EOS of dense nuclear medium from the nuclear experiments in terrestrial laboratories are not always consistent with the constraints from the astronomical observations of compact stars.

Recently, there have been successively reported the noticeable astronomical observations that suggest the stiff EOS of NS matter. The first is the large radii $R = 13.7 \pm 0.6\,\mathrm{km}$ of the nearby isolated neutron star RX J1856.5-3754 [1] with the assumed gravitational mass $M_G = 1.5M_\odot$ and $R = 14.5^{+1.8}_{-1.6}\,\mathrm{km}$ of a NS in qLMXB X7 [2] with the assumed gravitational mass $M_G = 1.4M_\odot$. Although their masses have not been confirmed yet, they suggests strongly that the radii of typical NSs with their masses $1.4M_\odot \leq M_G \leq 1.5M_\odot$ are larger than 13 km. The second is the massive NSs of $M_G = 2.1 \pm 0.2M_\odot$ [31] in the millisecond pulsar PSR J0751+1807 and $M_G = 2.44 \pm 0.27M_\odot$ [32] in the X-ray binary 4U1700-37. We show in Fig. 4 the mass-radius relations of NSs in the EZM models as well as these data. The maximum gravitational masses $M_G = 2.18M_\odot$ in the EZM1 and $M_G = 2.17M_\odot$ in the EZM2 lie just on the lower limit of 4U1700-37. It is seen that both

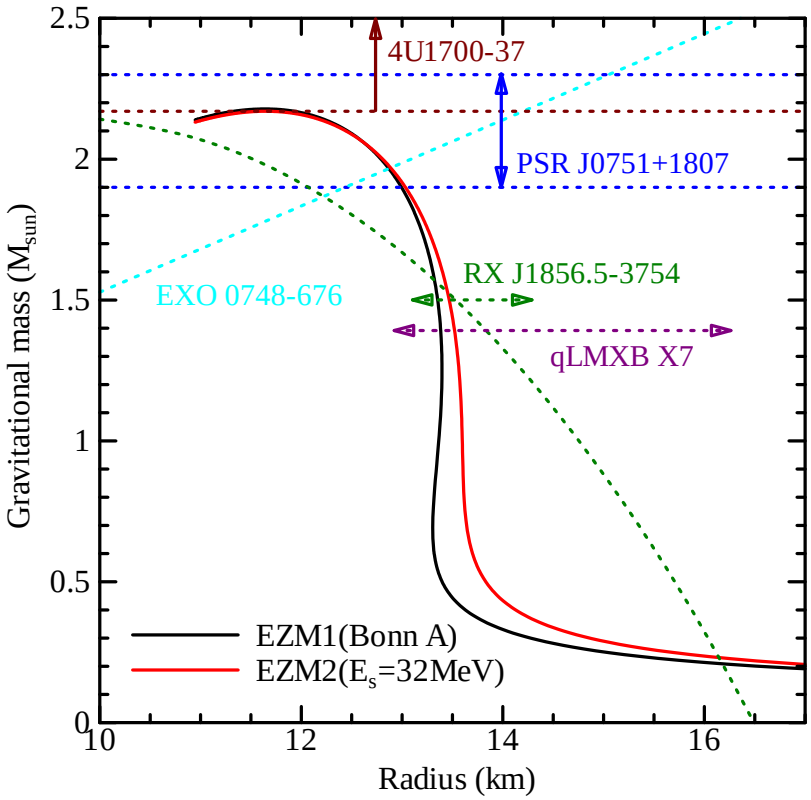

Figure 4: The mass-radius relations of NSs in the EZM1 (the black curve) and the EZM2 (the red curve) along with the observational data of several NSs.

the EZM models satisfy all of the constraints on the mass-radius relation of NS. On the other hand, the work [33] derived another constraint on RX J1856.5-3754 depicted by the green dotted curve in Fig. 4. Although it does not agree with the observation in Ref. [1], the larger radius than the EZM models is estimated for $M_G = 1.4M_\odot$. In any case, the observations of RX J1856.5-3754 suggest the stiff EOS of NS matter. Finally, the observed redshift $z = 0.35$ of EXO 0748-676 [34] also offers a significant constraint on the mass-radius relation depicted by the light-blue dotted line in Fig. 3. According to the result, the EZM models predict a massive NS of $M_G \simeq 2.0M_\odot$ in EXO 0748-676. Although its mass or radius has not been well determined [35], such a high-mass is expected because we have already discovered the massive NSs in X-ray binaries as 4U1700-37 [32], 4U1636-536 [36] and Vela X-1 [37].

The recently discovered binary NS system J0737-3039 [38,39] has attracted considerable attention. It has been strongly expected [40-42] that even a moderately accurate measurement of the moment-of-inertia of the pulsar A is able to provide a strong constraint on the EOS of NS matter. On the other hand, Ref. [43] has estimated the baryonic mass of the pulsar B, which also strongly constrains the EOS because its gravitational mass [39] is well determined. Unfortunately, none of the RMF models in Ref. [5] can satisfy the constraint while the EOS from the variational calculation [3] is satisfactory. This

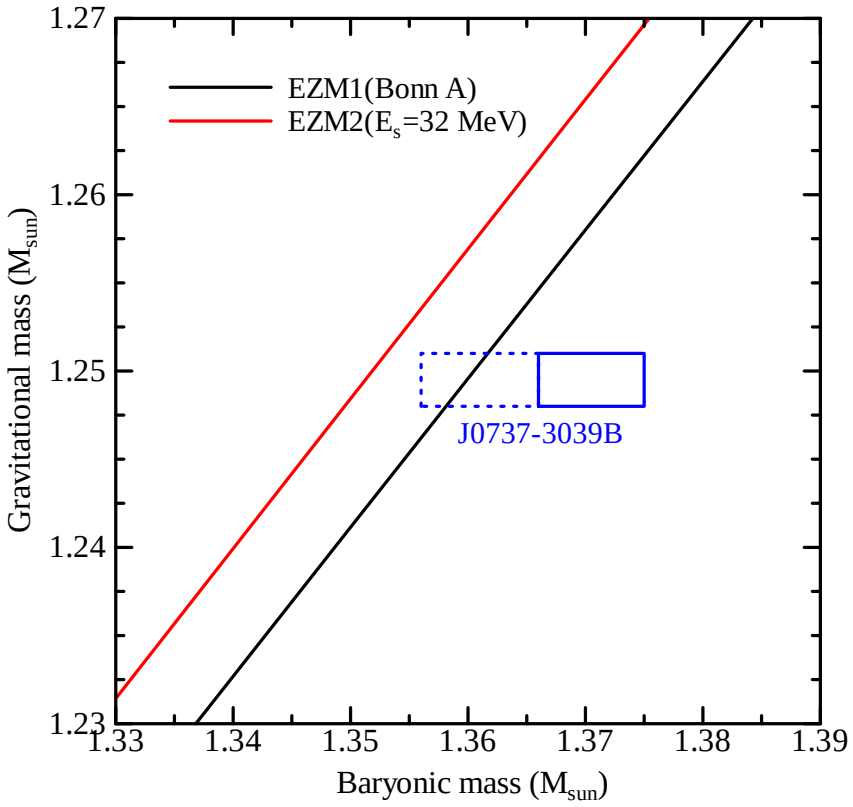

Figure 5: The gravitational-baryonic mass relation of NSs. The black and red curves are the results of EZM1 and EZM2, respectively. The rectangles enclosed by the solid and dotted blue lines are the constraints from J0737-3039B in Refs. [43] and [5], respectively.

is sharply contrast to the above results from X-ray binaries that exclude the variational model. It is however noted that the constraint is critically based on the assumption of the formation scenario for the pulsar B. Then, Ref. [5] assumed the loss of baryon number by 1% of the solar mass. The black and red solid curves in Fig. 5 show the results of gravitational-baryonic mass relations in EZM1 and EZM2, respectively. The rectangle enclosed by the solid blue lines is the constraint of Ref. [43] while the rectangle enclosed by the dotted blue lines is due to Ref. [5]. Although the strong constraint of Ref. [43] can never be satisfied, the EZM1 meets the weak constraint of Ref. [5].

4 Summary and conclusions

Recently, T. Klähn, *et al.* [5] has tested the several kinds of RMF models against the empirical information of EOS for dense nuclear matter from the heavy-ion reactions in terrestrial laboratories and the compact stars in universe. The present work supplements them with adding the tests of the EZM model, which is a truly nonlinear RMF model based on the constituent quark picture of nucleons. The two sets of $NN\rho$ coupling constant are considered. The first is the same as the Bonn A potential while the second

Table 2: Summary of results for the proposed scheme of tests.

	$L = 88 \pm 22$ MeV	Direct URCA	J1856.5-3754	qLMXB X7	PSR J0751+1807	4U1700-37	J0737-3039B	No. of passed tests
NLρ	◯	×	×	×	×	×	×	1
NL$\rho\delta$	◯	×	×	◯	×	×	×	2
DBHF	◯	×	×	×	◯	◯	◯	4
DD	×	◯	◯	◯	◯	◯	×	5
D3C	×	◯	◯	◯	◯	◯	×	5
KVR	×	◯	×	×	×	×	◯	2
KVOR	◯	◯	×	×	◯	×	×	3
DD-F	×	◯	×	×	◯	×	◯	3
EZM1	×	◯	◯	◯	◯	◯	◯	6
EZM2	◯	×	◯	◯	◯	◯	×	5

is chosen so as to reproduce the symmetry energy $E_s = 32\,\mathrm{MeV}$ of nuclear matter. The contents of tests are the following: 1) The constraint on the pressure of NS matter from the flow data of heavy-ion reactions; 2) The constraint $L = 88 \pm 22\,\mathrm{MeV}$ on the density dependence of the symmetry energy; 3) The direct URCA constraint $M_G^{DU} \geq 1.5M_\odot$ on the gravitational mass of NS; 4) The constraint $R = 13.7 \pm 0.6\,\mathrm{km}$ on radius of the isolated NS RX J1856.5-3754 with the assumed gravitational mass $M_G = 1.5M_\odot$; 5) The second constraint $R = 14.5^{+1.8}_{-1.6}\,\mathrm{km}$ on radius of a NS in qLMXB X7 with the assumed gravitational mass $M_G = 1.4M_\odot$; 6) The constraint $M_G = 2.1 \pm 0.2M_\odot$ on mass of a NS in the millisecond pulsar PSR J0751+1807; 7) The second constraint $M_G = 2.44 \pm 0.27M_\odot$ on mass of a compact star in the X-ray binary 4U1700-37; 8) The constraint on baryonic mass from J0737-3039B:

The results are summarized in Table 2. The results of the other RMF models than the EZM models are from Ref. [5]. We have omitted the test 1 because Ref. [5] tested the EOS of symmetric nuclear matter but not of NS matter. For the test 8 we assume the weak constraint suggested in Ref. [5] because none of the RMF models can satisfy the strong constraint of Ref. [43]. For the number of the passed tests, the DD and EZM models are good. Especially, the EZM1 is the best one. It is however noted that the proposed tests are not always consistent to each other. In fact, the test 2 is not consistent to the test 3 except for the KVOR. Moreover, we have to note that there remain uncertainties in the information from compact stars while the information from heavy-ion reactions strongly depend on the model of numerical simulation.

We can see that our result is different from Table V in Ref. [5]. In fact, our valuation

on the KV models is low in contrast to Ref. [5]. This is because the contents of both the tests are somewhat different from each other. We have omitted the constraint on the incompressibility while Ref. [5] omitted the constraint on the symmetry energy. However, the recent analysis [44] of K^+ production in heavy-ion reactions has predicted rather low incompressibility $K \simeq 200\,\mathrm{MeV}$ and so excludes the KV models. Moreover, if the constraint $M_N^* \simeq 0.6 M_N$ [45,46] on the effective mass of nucleon at saturation is taken into account, our valuation on the KV models becomes lower. The common result to both the investigations is that the NLW model is not suitable for NS matter. Although we can adjust the parameters in NLW model [47,48] so as to pass any test in Table 2, the NLW model with the accurately calibrated set of parameters in Ref. [49] predicts the similar results to the NLρ and NL$\rho\delta$ in Table 2. It is noted again that unlike the KV and the EZM models the NLW model is not a truly nonlinear RMF model. The implicit or explicit density dependences of the meson-nucleon coupling constants realized in the DD, KV and EZM models are crucial to studying the dense nuclear matter

In spite of the incompleteness of our tests, we can see that the EZM models have unique and excellent features. For the nuclear matter saturation properties, the EZM model predicts the same results [14] as the DBHF in Ref. [15]. The EZM2 and the NLW models are able to reproduce the density dependence of the symmetry energy. Only the DD and EZM models predict large radius $R > 13\,\mathrm{km}$ of NSs with typical gravitational mass $1.4 M_\odot \leq M_G \leq 1.5 M_\odot$. For the baryonic mass constraint from J0737-3039B, the EZM1 has a common advantage to the KV model. It is however important to note that the EZM1 has no parameters in the isovector contributions. Even the EZM2 has only three parameters in contrast to the NLW, DD and KV models. In this respect the EZM model can be regarded as a semi-microscopic model. Consequently, we can conclude that the EZM model is the most promising model for NS matter.

In the present work, we have taken into account nucleons only as baryons for the comparison with the results of Ref. [5]. It is however well known [50] that the hyperons may appear in the inner cores of NSs and soften the EOS of NS matter at high densities considerably. In this case, although the nucleon-hyperon and hyperon-hyperon interactions have not been well determined, the maximum gravitational mass of NS is $M_G \simeq 1.6 M_\odot$ [20] and so the above tests 6 and 7 cannot be passed. It is necessary to go beyond the EZM model so as to reproduce the massive NSs. We will challenge to the subject in future works.

Appendix: Table of the EOSs

For the reproduction of our results we here tabulate the EOSs, the pressure P vs. the baryon density ρ_B and the energy density $\mathcal{E}$, of the EZM models in the core region $\rho_B \geq 0.08\,\mathrm{fm}^{-3}$ of NSs. For the crust we have used the EOSs in Ref. [30].

	EZM1		EZM2	
$\rho_B(\mathrm{cm}^{-3})$	$\mathcal{E}(\mathrm{g}\cdot\mathrm{cm}^{-3})$	$P(\mathrm{dyn}\cdot\mathrm{cm}^{-2})$	$\mathcal{E}(\mathrm{g}\cdot\mathrm{cm}^{-3})$	$P(\mathrm{dyn}\cdot\mathrm{cm}^{-2})$
8.00E+37	1.341722E+14	3.508627E+32	1.347333E+14	7.477153E+32
1.00E+38	1.678871E+14	9.968690E+32	1.687182E+14	1.543051E+33
1.20E+38	2.017903E+14	2.075634E+33	2.029242E+14	2.764063E+33
1.40E+38	2.359388E+14	3.671253E+33	2.374003E+14	4.469768E+33
1.60E+38	2.703856E+14	5.857574E+33	2.721841E+14	6.654859E+33
1.80E+38	3.051795E+14	8.668718E+33	3.073098E+14	9.410959E+33
2.00E+38	3.403584E+14	1.211220E+34	3.428143E+14	1.280443E+34
2.20E+38	3.759586E+14	1.626001E+34	3.787339E+14	1.689154E+34
2.40E+38	4.120154E+14	2.115888E+34	4.151036E+14	2.172183E+34
2.60E+38	4.485624E+14	2.684685E+34	4.519568E+14	2.733862E+34
2.80E+38	4.856307E+14	3.335562E+34	4.893254E+14	3.377900E+34
3.00E+38	5.232494E+14	4.071111E+34	5.272393E+14	4.107385E+34
3.20E+38	5.614455E+14	4.893388E+34	5.657264E+14	4.924781E+34
3.40E+38	6.002438E+14	5.803937E+34	6.048129E+14	5.831950E+34
3.60E+38	6.396670E+14	6.803817E+34	6.445226E+14	6.830175E+34
3.80E+38	6.797359E+14	7.893636E+34	6.848775E+14	7.920202E+34
4.00E+38	7.204692E+14	9.073586E+34	7.258975E+14	9.102288E+34
4.20E+38	7.618839E+14	1.034349E+35	7.676005E+14	1.037625E+35
4.40E+38	8.039950E+14	1.170283E+35	8.100027E+14	1.174154E+35
4.60E+38	8.468159E+14	1.315082E+35	8.531182E+14	1.319729E+35
4.80E+38	8.903585E+14	1.468642E+35	8.969594E+14	1.474235E+35
5.00E+38	9.346330E+14	1.630840E+35	9.415374E+14	1.637538E+35
5.20E+38	9.796483E+14	1.801537E+35	9.868614E+14	1.809488E+35
5.40E+38	1.025412E+15	1.980583E+35	1.032939E+15	1.989920E+35
5.60E+38	1.071930E+15	2.167816E+35	1.079778E+15	2.178663E+35
5.80E+38	1.119209E+15	2.363072E+35	1.127383E+15	2.375540E+35
6.00E+38	1.167251E+15	2.566178E+35	1.175758E+15	2.580370E+35
6.20E+38	1.216061E+15	2.776963E+35	1.224908E+15	2.792969E+35
6.40E+38	1.265642E+15	2.995252E+35	1.274835E+15	3.013157E+35
6.60E+38	1.315994E+15	3.220873E+35	1.325539E+15	3.240752E+35
6.80E+38	1.367119E+15	3.453654E+35	1.377024E+15	3.475575E+35
7.00E+38	1.419017E+15	3.693425E+35	1.429289E+15	3.717451E+35
7.20E+38	1.471688E+15	3.940018E+35	1.482333E+15	3.966208E+35
7.40E+38	1.525132E+15	4.193270E+35	1.536157E+15	4.221676E+35

	EZM1		EZM2	
$\rho_B(\mathrm{cm}^{-3})$	$\mathcal{E}(\mathrm{g}\cdot\mathrm{cm}^{-3})$	$P(\mathrm{dyn}\cdot\mathrm{cm}^{-2})$	$\mathcal{E}(\mathrm{g}\cdot\mathrm{cm}^{-3})$	$P(\mathrm{dyn}\cdot\mathrm{cm}^{-2})$
7.60E+38	1.579347E+15	4.453020E+35	1.590759E+15	4.483690E+35
7.80E+38	1.634332E+15	4.719109E+35	1.646137E+15	4.752088E+35
8.00E+38	1.690085E+15	4.991381E+35	1.702290E+15	5.026711E+35
8.20E+38	1.746603E+15	5.269687E+35	1.759216E+15	5.307407E+35
8.40E+38	1.803885E+15	5.553875E+35	1.816911E+15	5.594022E+35
8.60E+38	1.861928E+15	5.843802E+35	1.875373E+15	5.886410E+35
8.80E+38	1.920728E+15	6.139322E+35	1.934599E+15	6.184424E+35
9.00E+38	1.980282E+15	6.440296E+35	1.994586E+15	6.487923E+35
9.20E+38	2.040587E+15	6.746585E+35	2.055330E+15	6.796767E+35
9.40E+38	2.101640E+15	7.058053E+35	2.116827E+15	7.110817E+35
9.60E+38	2.163435E+15	7.374565E+35	2.179074E+15	7.429939E+35
9.80E+38	2.225970E+15	7.695988E+35	2.242066E+15	7.753996E+35
1.00E+39	2.289241E+15	8.022189E+35	2.305800E+15	8.082858E+35
1.02E+39	2.353242E+15	8.353039E+35	2.370270E+15	8.416392E+35
1.04E+39	2.417970E+15	8.688408E+35	2.435473E+15	8.754467E+35
1.06E+39	2.483421E+15	9.028164E+35	2.501405E+15	9.096953E+35
1.08E+39	2.549589E+15	9.372179E+35	2.568060E+15	9.443718E+35
1.10E+39	2.616470E+15	9.720323E+35	2.635433E+15	9.794633E+35
1.12E+39	2.684060E+15	1.007246E+36	2.703521E+15	1.014956E+36
1.14E+39	2.752354E+15	1.042847E+36	2.772318E+15	1.050838E+36
1.16E+39	2.821346E+15	1.078821E+36	2.841819E+15	1.087094E+36
1.18E+39	2.891031E+15	1.115153E+36	2.912019E+15	1.123711E+36
1.20E+39	2.961405E+15	1.151831E+36	2.982912E+15	1.160674E+36

References

[1] T.M. Braje and R.W. Romani, Astrophys. J. **580** (2002) 1043.

[2] G.B. Rybicki, C.O. Heinke, R. Narayan and J.E. Grindlay, arXiv:astro-ph/0506563.

[3] A. Akmal, V.R. Pandharipande and D.G. Ravenhall, Phys. Rev. C **58** (1998) 1804 [arXiv:nucl-th/9804027].

[4] B.D. Serot and J.D. Walecka, *Advances in Nuclear Physics*, Vol. **16** (Plenum, New York, 1986).

[5] T. Klähn, *et al.*, arXiv:nucl-th/0602038.

[6] B. Liu, V. Greco, V. Baran, M. Colonna and M. Di Toro, Phys. Rev. C **65** (2002) 045201 [arXiv:nucl-th/0112034].

[7] C. Fuchs, Lect. Notes Phys. **641** (2004) 119 [arXiv:nucl-th/0309003].

[8] S. Typel, Phys. Rev. C **71** (2005) 064301 [arXiv:nucl-th/0501056].

[9] E.E. Kolomeitsev and D.N. Voskresensky, Nucl. Phys. A **759** (2005) 373 [arXiv:nucl-th/0410063].

[10] J. Zimanyi and S.A. Moszkowski, Phys. Rev. C **42** (1990) 1416.

[11] K. Miyazaki, Prog. Theor. Phys. **93** (1995) 137.

[12] K. Miyazaki, Prog. Theor. Phys. **91** (1994) 1271.

[13] K. Miyazaki, Mathematical Physics Preprint Archive (mp_arc) 05-141.

[14] K. Miyazaki, Mathematical Physics Preprint Archive (mp_arc) 05-178.

[15] R. Brockmann and R. Machleidt, Phys. Rev. C **42** (1990) 1965.

[16] K. Miyazaki, Mathematical Physics Preprint Archive (mp_arc) 05-190.

[17] K. Miyazaki, Mathematical Physics Preprint Archive (mp_arc) 05-199.

[18] K. Miyazaki, Mathematical Physics Preprint Archive (mp_arc) 05-206.

[19] K. Miyazaki, Mathematical Physics Preprint Archive (mp_arc) 05-216.

[20] K. Miyazaki, Mathematical Physics Preprint Archive (mp_arc) 05-224.

[21] K. Miyazaki, Mathematical Physics Preprint Archive (mp_arc) 05-233.

[22] K. Miyazaki, Mathematical Physics Preprint Archive (mp_arc) 06-91.

[23] K. Miyazaki, Mathematical Physics Preprint Archive (mp_arc) 05-427.

[24] C.-H. Lee, T.T.S. Kuo, G.Q. Li and G.E. Brown, arXiv:nucl-th/9703034.

[25] B-A. Li, L-W. Chen, C.M. Ko, G-C. Yong and W. Zuo, arXiv:nucl-th/0504009; B-A. Li, L-W. Chen, C.M. Ko and A.W. Steiner, arXiv:nucl-th/0601028.

[26] P. Danielewicz, R. Lacey and W.G. Lynch, Science **298** (2002) 1592 [arXiv:nucl-th/0208016].

[27] L-W. Chen, C.M. Ko and B-A. Li, Phys. Rev. C **72** (2005) 064309 [arXiv:nucl-th/0509009].

[28] B-A. Li and L-W. Chen, Phys. Rev. C **72** (2005) 064611 [arXiv:nucl-th/0508024].

[29] W.D. Arnett and R.L. Bowers, Astrophys. J. Suppl. **33** (1977) 415.

[30] V. Canuto, Ann. Rev. Astr. Ap. **12** (1974) 167; **13** (1975) 335.

[31] D.J. Nice *et al.*, arXiv:astro-ph/0508050.

[32] J.S. Clark *et al.*, Astron. Astrophys. **392** (2002) 909.

[33] J.E. Trümper, V. Burwitz, F. Haberl and V.E. Zavlin, arXiv:astro-ph/0312600.

[34] J. Cottam, F. Paerels and M. Mendez, Nature **420** (2002) 51 [arXiv:astro-ph/0211126].

[35] A.R. Villarreal and T.E. Strohmayer, Astrophys. J. **614** (2004) L121 [arXiv:astro-ph/0409384].

[36] D. Barret, J-F. Olive, M.C. Miller, Mon. Not. Roy. Astron. Soc. **361** (2005) 855 [arXiv:astro-ph/0505402].

[37] H. Quaintrell *et al.*, Astron. Astrophys. **401** (2003) 313 [arXiv:astro-ph/0301243].

[38] M. Burgay *et al.*, Nature **426** (2003) 531 [arXiv/astro-ph/0312071].

[39] A.G. Lyne *et al.*, Science **303** (2004) 1153 [arXiv:astro-ph/0401086].

[40] I.A. Morrison, T.W. Baumgarte, S.L. Shapiro and V.R. Pandharipande, Astrophys. J. **617** (2004) L135 [arXiv:astro-ph/0411353].

[41] J.M. Lattimer and B.F. Schutz, Astrophys. J. **629** (2005) 979 [arXiv:astro-ph/0411470].

[42] M. Bejger, T. Bulik and P. Haensel, Mon. Not. Roy. Astron. Soc. **364** (2005) 635 [arXiv:astro-ph/0508105].

[43] Ph. Podsiadlowski, J.D.M. Dewi, P. Lesaffre, J.C. Miller, W.G. Newton and J.R. Stone, Mon. Not. Roy. Astron. Soc. **361** (2005) 1243 [arXiv:astro-ph/0506566].

[44] Ch. Hartnack, H. Oeschler and J. Aichelin, Phys. Rev. Lett. **96** (2006) 012302 [arXiv:nucl-th/0506087].

[45] W. Koepf, M.M. Sharma and P. Ring, Nucl. Phys. A **533** (1991) 95.

[46] M.M. Sharma, M.A. Nagarajan and P. Ring, Ann. of Phys. **231** (1994) 110.

[47] C.J. Horowitz and J. Piekarewicz, Phys. Rev. C **66** (2002) 055803 [arXiv:nucl-th/0207067].

[48] J. Carriere, C.J. Horowitz and J. Piekarewicz, Astrophys. J. **593** (2003) 463.

[49] B.G. Todd-Rutel and J. Piekarewicz, Phys. Rev. Lett. **95** (2005) 122501 [arXiv:nucl-th/0504034].

[50] S. Balberg, I. Lichtenstadt and G.B. Cook, Astrophys. J. Suppl. **121** (1999) 515.